A Density Functional Study of Phosphorus Nitride P_3N_5: Refined Geometries, Properties, and Relative Stability of α-P_3N_5 and γ-P_3N_5 and a Further Possible High-Pressure Phase δ-P_3N_5 with Kyanite-Type Structure

Peter Kroll*[a] and Wolfgang Schnick*[b]

Abstract: The crystal structures and the enthalpy–pressure phase diagram of P_3N_5 were investigated by using density functional methods. Applying both approximations to the electron exchange and correlation gives a consistent picture for the two known polymorphs, α-P_3N_5 and γ-P_3N_5. The calculated zone-center phonon modes compare very well with the experimental results. They indicate low-frequency bending modes for two-coordinate N atoms of α-P_3N_5, which are responsible for a $C2/c \rightarrow Cc$ structural modulation of α-P_3N_5 at moderate pressures. α-P_3N_5 transforms into γ-P_3N_5 at pressures of about 6 GPa. We propose γ-P_3N_5 transforms into a δ-P_3N_5 with Kyanite-type structure at pressures exceeding 43 GPa. Upon quenching, this triclinic modification of P_3N_5 is likely to distort into a more symmetric monoclinic structure.

Keywords: density functional calculations · high-pressure synthesis · phase diagrams · phosphorus nitride

Introduction

The binary nonmetal nitrides BN and Si_3N_4 have become particularly significant for the preparation of high-performance materials with outstanding chemical, thermal, and mechanical stability.[1] Recently, phosphorus nitride P_3N_5 was structurally characterized after considerable effort.[2, 3] Similar to α- and β-Si_3N_4 as well as c-BN, α-phosphorus nitride is built up by a covalent network structure of $\{\mathbf{T}\}N_4$ tetrahedra ($\mathbf{T}$ = B, Si, P). The structure of α-P_3N_5 is drawn in Figure 1. However, contrary to c-BN and α- and β-Si_3N_4, the $\{\mathbf{P}\}N_4$ tetrahedra in α-P_3N_5 are linked through both common corners and common edges.

The development of modern high-pressure techniques recently led to the discovery of spinel-type γ-Si_3N_4.[4, 5] According to the pressure coordination rule the coordination number (CN) of Si was increased from four in α- and β-Si_3N_4, to four and six in spinel-type γ-Si_3N_4, representing one of the very rare examples of Si octahedrally coordinated by nitrogen, found to date.

Very recently a novel high-pressure polymorph of phosphorus nitride, γ-P_3N_5, was characterized, which similar to γ-Si_3N_4 exhibits an increase in the coordination number of phosphorus as compared with α-P_3N_5.[6] The structure of γ-P_3N_5 is given in Figure 2. Tetrahedral $\{\mathbf{P}\}N_4$ and distorted square-pyramidal $\{\mathbf{P}\}N_5$ units were detected in a molar ratio of 1:2 in the high-pressure polymorph γ-P_3N_5. From these experimental findings the question arose concerning the accurate electronic structure of both phosphorus nitrides and their relative stabilities. Furthermore, since modern high-pressure solid-state chemistry using either static diamond-anvil cell techniques[7] or dynamic shock compression methods[8] is able to produce pressures of 50–200 GPa and beyond, the possibility of a transformation to a further high-pressure polymorph with octahedral $\{\mathbf{P}\}N_6$ groups warrants investigation.

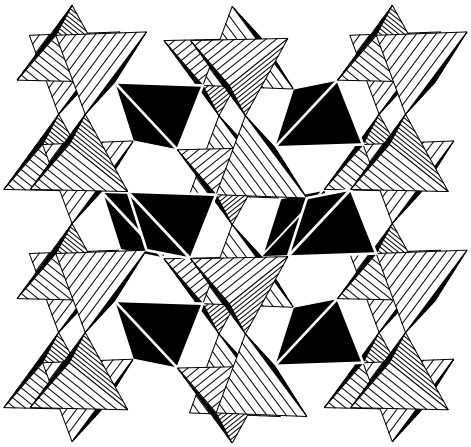

Figure 1. The structure of α-P_3N_5. All P atoms are tetrahedrally coordinated. Hatched tetrahedra refer to edge-sharing tetrahedra, black tetrahedra to those sharing vertices only.

[a] Dr. P. Kroll
Institut für Anorganische Chemie der RWTH Aachen
Professor-Pirlet-Strasse 1, 52056 Aachen (Germany)
Fax: (+49) 241 80-92288
E-mail: peter.kroll@ac.rwth-aachen.de

[b] Prof. Dr. W. Schnick
Department Chemie der Ludwig-Maximilians-Universität
Butenandtstrasse 5–13 (Haus D), 81377 München (Germany)
Fax: (+49) 89 2180-7440
E-mail: wolfgang.schnick@uni-muenchen.de

  0947-6539/02/0815-3530 $ 20.00+.50/0

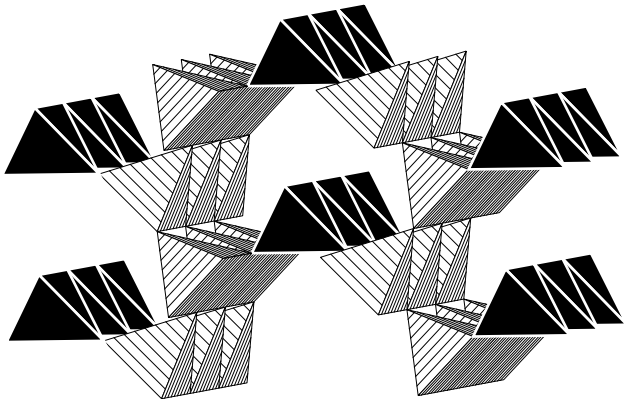

Figure 2. The structure of γ-P_3N_5. Tetrahedra are colored black, square pyramids are hatched.

Computational Methods

We calculated the total energies, atomic structures, and atomic dynamics by using density functional theory (DFT).[9] The implementation of DFT employed here combines a plane-wave basis set with the total energy pseudopotential method. In particular we used the Vienna Ab initio Simulation Package (VASP).[10, 11, 12] The exchange-correlation energy of the electrons is treated within the local density approximation (LDA) as parametrized by Perdew and Zunger[13] based on results of Ceperley and Alder.[14] In addition, we used the generalized-gradient approximation (GGA) of Perdew and Wang.[15]

Structures of P_3N_5 were completely optimized by using a cut-off of 400 eV for the expansion of the wavefunction into the plane wave basis set. For the integration over the Brillouin zone we used the scheme developed by Monkhorst and Pack.[16] A $2 \times 4 \times 2$ mesh resulted in four special **k** points for the *C*2/*c* or *Cc* space group symmetry of α-P_3N_5. For γ-P_3N_5, space group *I*22*m*, a $2 \times 8 \times 4$ mesh resulted in eight special **k** points. Forces were relaxed to values below 10^{-2} eV Å^{-1} and stresses below 1 kbar. Using finer grids for the **k** point sampling, or larger plane wave basis sets confirmed the convergence of structural properties at this level of accuracy. The total energy differences are found to be converged to values of 0.01 eV per formula unit of P_3N_5 (about 1 meV per atom). The zone-center phonon frequencies of α-P_3N_5 and γ-P_3N_5 were calculated by using primitive unit cells. The Monkhorst – Pack meshes were appropriately chosen, a $4 \times 4 \times 2$-mesh for α-P_3N_5 and a $4 \times 4 \times 4$-mesh for γ-P_3N_5.

A comparison of LDA and GGA results provides useful guidelines. For structures of main-group elements the LDA typically underestimates the lattice volume by 1–3%, while the GGA overestimates volumes by 3–8%. Elastic properties of such compounds are usually described very well within the LDA, while the GGA underestimates compressibility and elastic constants by 10–20%. On the other hand, it has been documented that gradient corrections offer significant improvements when structures with different environments for the atoms are compared with each other, especially for the estimation of transition pressures. Since we encounter such a situation in our study, we will make use of both approximations to the electron-electron interaction.

Abstract in German: *Die Kristallstrukturen sowie das Enthalpie-Druck Phasendiagramm von P_3N_5 wurden mit Dichtefunktionalmethoden untersucht. Die Anwendung beider Approximationen zur Austausch- und Korrelationsenergie der Elektronen lieferte ein konsistentes Bild für beide Polymorphe, α-P_3N_5 und γ-P_3N_5. Die berechneten Phononmoden entsprechen weitgehend den experimentellen Ergebnissen. Für α-P_3N_5 lassen sich niederfrequente Beugungsmoden der zweifach koordinierten Stickstoffatome identifizieren, die für eine Strukturmodulation von C2/c nach Cc bereits bei geringen Drücken verantwortlich sind. Der berechnete Druck für die Transformation α-P_3N_5 nach γ-P_3N_5 beträgt 6 GPa. Die Ergebnisse lassen desweiteren die Existenz eines δ-P_3N_5 mit Kyanitstruktur vermuten, welches bei Drücken jenseits von 43 GPa gebildet werden sollte. Diese trikline Modifikation sollte beim Abschrecken in eine höher-symmetrische monokline Modifikation transformieren.*

Results and Discussion

α-P_3N_5: The data of the optimized crystal structure of α-P_3N_5 are given in Table 1. Apparently, the LDA underestimates the cell volume by 1%, while the GGA overestimates it by 2.5% in comparison to the experimental value. The overall proportions of the cell geometry, ratios of lattice constants and the angle β, are, however, in an excellent agreement with the experimental values reported in reference [2]. Interestingly, our calculations of the crystal structure of α-P_3N_5 always converged towards the *C*2/*c* space group, when using the experimental data within the space group *Cc* as the starting geometry. It is worth mentioning that the energy difference between the two settings of α-P_3N_5, taking equal cell contants, is only small ($\approx$0.1 eV/P_3N_5) and not much higher than the reliability of the computational method. The calculated forces, however, provide a clear indicator. For the experimental positions of the *Cc* setting we found forces of up to 0.3 eV Å^{-1} at the N1 and P3 position, a value which is one order of magnitude above our convergence criterion of 10^{-2} eV Å^{-1}. Moreover, we made several attempts to confirm the *C*2/*c* space group for α-P_3N_5, including random displacements of the original positions, symmetry reduction to *P*1 and/or cell shape distortion. In every case, however, our calculation ended up with the space group geometry with the additional inversion center. We are, therefore, confident of *C*2/*c* being the true space group of α-P_3N_5. The calculated zone-center phonon modes (see below) corroborate this result.

Table 1. Space group symmetry, lattice constants, and volume (per formula unit P_3N_5) of α-P_3N_5 calculated within LDA and GGA. For comparison the experimental results (standard deviations in parentheses) are taken from ref. [2].

	LDA	GGA	Exp.
space group (no.)	*C*2/*c* (15)	*C*2/*c* (15)	*Cc* (9)
a [Å]	8.098	8.179	8.12077(4)
b [Å]	5.822	5.892	5.83433(4)
c [Å]	9.134	9.229	9.16005(5)
β	116.0	115.7	115.809(1)
V [Å^3]	96.8	100.2	97.7

A consequence of the higher symmetrical arrangement of α-P_3N_5 is a linear coordinated N atom (P-N-P angle of 180°) at the center of inversion. The energy potential associated with the bond angle, however, appears to be very shallow as suggested by the small energy difference towards the less symmetrical setting. The analysis of the eigenvectors of the vibrational modes given in a subsequent section furthermore

  0947-6539/02/0815-3531 $ 20.00+.50/0

indicates that this N atom, located at the center of inversion, takes part in several low-frequency phonon modes, and thus is prone to distortions. We encounter this structural instability of α-P_3N_5 when pressure is applied to the structure (see below). We regard our results not to be in contradiction to the experiment, but more to be an additional refinement of the structure of α-P_3N_5. Previously, we had already discussed the possibility of the centrosymmetric space group.[3] However, at that time the experimental data did not allow an unambiguous assignment, presumably due to a certain amount of structural disorder, arising from stacking faults and twinning, as well as contamination with β-P_3N_5.

The calculated atomic positions of α-P_3N_5 are given in Table 2, the experimental data determined from synchrotron powder diffraction is listed in Table 3. The specific setting we used for the experimental data within space group *Cc* already

Table 2. Atomic positions of α-P_3N_5 obtained within LDA and GGA.

	LDA			GGA		
Atom	*x*	*y*	*z*	*x*	*y*	*z*
P1	½	0.0174	¼	½	0.0208	¼
P2	0.3658	0.2962	0.4447	0.3695	0.3004	0.4430
N1	0	0	0	0	0	0
N2	0.3705	0.1387	0.3099	0.3775	0.1461	0.3090
N3	0.1446	0.3552	0.3999	0.1473	0.3567	0.3964

Table 3. Experimentally determined atomic coordinates of α-P_3N_5 in space group *Cc*.[2] [a]

Atom	*x*	*y*	*z*
P1	½	0.0182(3)	¼
P2	0.636(1)	0.7000(8)	0.559(1)
P3	0.365(2)	0.2924(8)	0.446(1)
N1	0.009(2)	0.003(2)	0.019(1)
N2	0.629(1)	0.841(1)	0.700(1)
N3	0.370(1)	0.119(1)	0.316(1)
N4	0.142(2)	0.351(2)	0.397(1)
N5	0.856(2)	0.635(2)	0.598(1)

[a] All atoms are in Wyckoff positions 4a. Standard deviations are given in parentheses. The coordinates $P1_x$ and $P1_z$ were fixed during the refinement. Note that in comparison to the work reported in reference [2], we shifted the coordinates by a translational vector of [0,0,¼]. Doing so hints at the approximate inversion symmetry, which relates the atom pairs P2/P3, N2/N3, and N4/N5. Moreover, N1 gets close to the origin of the coordinate system, which in *C*2/*c* is the center of inversion (Wyckoff position 2a).

hints at the approximate inversion symmetry. A comparison of experimental and theoretical data shows a very good agreement. The data can furthermore be used to calculate bond lengths and angles for each atom. In Table 4 we list the

Table 4. Comparison of average N–P bond lengths of two- and three-coordinate N atoms in calculated and experimental structures of α-P_3N_5. Numbers in brackets denote the respective standard deviation.

Average bond lengths	LDA	GGA	Exp.
$N^{[2]}$–P	1.545 (0.007)	1.558 (0.006)	1.555 (0.031)
$N^{[3]}$–P	1.682 (0.026)	1.703 (0.027)	1.690 (0.038)

average bond lengths for N–P bonds for two-coordinate and three-coordinate N atoms, denoted $N^{[2]}$ and $N^{[3]}$, together with the respective standard deviation. Bond lengths of similar coordinated N atoms are significantly more consistent within the calculated structures than they are within the refined structure based on powder diffraction data. For example, within the LDA the N–P bond lengths of two-coordinate N atoms vary by only 0.01 Å, between 1.537 and 1.549 Å. In comparison, the experimentally derived bond lengths vary much more between 1.507 and 1.599 Å. This trend is somewhat smaller for the N–P bond lengths of three-coordinate N atoms, which vary between 1.653 and 1.704 Å within the LDA (experimental values vary between 1.639 and 1.745 Å). Some of these bonds are found within the P–N 4-rings of the structure and are presumably elongated due to a certain amount of ring strain. Overall, we obtain a more homogenous and consistent picture of α-P_3N_5 from the theoretical calculations, and take the observed deviations between calculated and experimentally determined structures as a further indication of residual structural disorder in the investigated powder samples.

γ-P_3N_5: Results of our calculations of the crystal structure of γ-P_3N_5 are given in Table 5 together with the experimental results from reference [6]. Quite similar to the situation for α-

Table 5. Lattice constants, and volume (per formula unit P_3N_5) of γ-P_3N_5 (γ-P_3N_5; space group, *Imm*2 (no. 44), $Z=2$) calculated within LDA and GGA in comparison to the experimental results from reference [6].

	LDA	GGA	Exp.
a [Å]	12.7874	13.0308	12.8720(5)
b [Å]	2.6053	2.6341	2.61312(6)
c [Å]	4.3512	4.4708	4.4004(2)
V [Å^3]	72.5	76.3	74.0

P_3N_5, the LDA underestimates the cell volume by 2%, while the GGA overestimates it by 3% in comparison to the experimental value. Table 6 lists the atomic positions of both calculated and experimental structures. The N–P bond lengths in γ-P_3N_5 are given in Table 7. Since γ-P_3N_5 contains

Table 6. Atomic positions of γ-P_3N_5 obtained within LDA and GGA in comparison to the experimental results of reference [6], space group *Imm*2. Standard deviations of the experimental values are given in parentheses.

		LDA			GGA			Exp		
atom	Wyckoff	*x*	*y*	*z*	*x*	*y*	*z*	*x*	*y*	*z*
P1	2a	0	0	0.3119	0	0	0.3022	0	0	0.3114(10)
P2	4c	0.3188	0	0.4508	0.3175	0	0.4571	0.3191(2)	0	0.4580(9)
N1	2b	½	0	0.0105	½	0	−0.0039	½	0	0.0159(15)
N2	4c	0.1038	0	0.0851	0.1040	0	0.0808	0.1047(4)	0	0.0768(9)
N3	4c	0.2768	½	0.2210	0.2750	½	0.2310	0.2735(6)	½	0.2196(12)

  0947-6539/02/0815-3532 $ 20.00+.50/0 *Chem. Eur. J.* **2002**, *8*, No. 15

Table 7. N–P bond lengths in calculated and experimental structures of γ-P_3N_5.

Bond lengths	LDA	GGA	Exp.
N1–P1	1.5632	1.5767	1.5864
N2–P1	1.6546	1.6782	1.6976
N2–P2	1.7369	1.7569	1.7153
N3–P2	1.6958	1.7183	1.6570
N3–P2	1.7279	1.7502	1.7753

not only $N^{[2]}$–$P^{[4]}$ and $N^{[3]}$–$P^{[4]}$, but two kinds of $N^{[3]}$–$P^{[5]}$ bond lengths, apical and basal within the square pyramids, as well, we can follow the intriguing trend of increasing bond lengths with increasing coordination of the respective atoms, N and P. This trend is well-known for many phases, covalent or metallic, and is sometimes termed the "pressure–bond length–paradoxon".[20] Overall, the calculated structures once more can be considered as an additional refinement of the structure of γ-P_3N_5. The theoretical results yield a consistent picture that enhances the experimental structure determination.

The vibrational spectra of α-P_3N_5 and γ-P_3N_5: The zone-center ($\mathbf{k}=0$) optical phonon modes provide information about the vibrational motions of the atoms in the crystal. The optical modes can be classified according to the irreducible representation of the space group and probed experimentally by IR and Raman absorption spectroscopy. For structures with an inversion center IR- and Raman-active modes are complementary. α-P_3N_5 and γ-P_3N_5 have space groups $C2/c$ and $Imm2$ with point groups C_{2h} and C_{2v}, respectively. Their zone-center optical phonons decompose according to Equations (1) and (2).

$$\Gamma_{opt} = 10A_g + 10A_u + 11B_g + 14B_u \qquad (\alpha\text{-}P_3N_5) \tag{1}$$

$$\gamma_{opt} = 7A_1 + 3A_2 + 7B_1 + 4B_2 \qquad (\gamma\text{-}P_3N_5) \tag{2}$$

Our calculations of zone-center phonon modes for α-P_3N_5 and γ-P_3N_5 are listed in Tables 8 and 9, respectively. For α-P_3N_5, whose primitive cell contains 16 atoms, we have a total of 45 (3.16–3) optical modes. According to group theoretical analysis, the inversion symmetry separates Raman- and IR-active modes. A_g and B_g are Raman-active modes, while A_u and B_u are IR-active. γ-P_3N_5, whose primitive cell contains just one formula unit (i.e. eight atoms), has in total 21 ($(3\times8)-3$) optical modes. The group theoretical analysis yields that all modes are Raman-active, but only A_1, B_1, and B_2 are IR-active.

Table 8. Zone-center phonon modes for α-P_3N_5. A_g and B_g are Raman-active modes, A_u and B_u are IR-active modes. The three pure translational modes transform according to A_u and $2B_u$.

A_g	A_u	B_g	B_u
1306	1362	1365	1359
1149	1316	1160	1278
826	1020	886	939
775	866	805	831
755	669	788	812
504	484	580	663
446	472	439	617
415	251	387	496
350	205	360	457
195	195	279	405
		176	320
			289
			207
			124

Table 9. Zone-center phonon modes for γ-P_3N_5. All modes are Raman-active. A_1, B_1, and B_2 are IR-active. The three pure translational modes transform according to A_1, B_1, and B_2.

A_1	A_2	B_1	B_2
1144	821	1157	1158
1003	591	933	757
859	318	698	645
619		670	267
537		512	
416		461	
271		292	
272			

Figure 3 shows the experimental IR spectra of α-P_3N_5 and γ-P_3N_5. These IR spectra characterize the vibrations by broad absorption lines, which is typical for solids and especially for powderous materials. Therefore, and due to the limited range of the IR spectrometer, not all 24 IR-active lines for α-P_3N_5 and all 18 lines for γ-P_3N_5 can be distinguished.

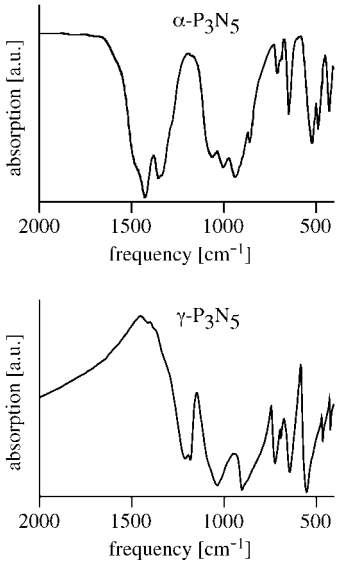

Figure 3. Experimental IR spectra of α-P_3N_5 (top) and γ-P_3N_5 (bottom).

The calculated vibrational modes of both structures are given in Table 8 and Table 9. Unfortunately, we can not access the oscillator strength of an individual mode and thus cannot determine which mode is expected to be weak or strong. However, the calculated wave numbers appear to be in reasonable agreement with the experimental data, although the calculated frequencies are somewhat lower (by $\approx 50\ cm^{-1}$) than the experimental maxima of absorption. Most evident, both for experimental and calculated spectra, is the significant shift to lower wave numbers of the principal mode in the IR spectra from α-P_3N_5 to γ-P_3N_5 by about $200\ cm^{-1}$. We calculated the highest IR-active frequency of α-P_3N_5 to be

1359 cm^{-1} and of γ-P_3N_5 to be 1157 cm^{-1}. This trend is consistent with the experimental results of 1420 cm^{-1} and 1200 cm^{-1} for α-P_3N_5 and γ-P_3N_5, respectively. We also find a significant "gap" in the IR spectrum of α-P_3N_5 between 1020 and 1278 cm^{-1}, which corresponds well with the experimental data.

Furthermore, the low-frequency part of the spectrum of α-P_3N_5 is worthy of note. With an analysis of the eigenvectors we can identify the two modes at 207 cm^{-1} (B_u) and 205 cm^{-1} (A_u) as (mainly) the (almost degenerate) bending mode for the P-N-P angle of the N atom at the inversion center. The low frequency indicates a low force constant for this bending mode—another indication that shows that α-P_3N_5 is prone to distortions from the *C*2/*c* space group symmetry towards *C*2, whether by dynamical disorder, by topological faults, or by impurities and defects.

The transition between α-P_3N_5 and γ-P_3N_5: The two polymorphs of P_3N_5 were further studied for their behavior under high pressure. The high-pressure experiment is simulated by a reduction of the unit cell volume of each structure. For both structures of α-P_3N_5 and γ-P_3N_5 we started from the optimized geometry ($p = 0$) and changed the volume of the unit cells stepwise by about 1.5%. For every volume, forces on atoms are relaxed and thus all atomic positions are optimized. For α-P_3N_5 the convergence criteria (residual forces ≤ 0.01 eV $Å^{-1}$) resulted in a large number of iterations, and thus high computational costs. A convergence criteria based on energy alone would not have given accurate results, and the reason for this is found in the shallow potential energy surface connected with the bending mode of two connected nitrogen atoms. We encountered a similar situation recently in silylated carbodiimide structures, which also exhibit two-coordinate N atoms.[21] The cell dimensions of α-P_3N_5 and γ-P_3N_5 were optimized as well under the constraint of constant volume, since except for cubic structures the linear compressibility is anisotropic in general. For example, the structure of γ-P_3N_5 responds rather anisotropically to the applied pressure: the lattice is more easily compressed in the *a* and *c* directions than it is in the *b* direction. Scaling only the lattice vectors isotropically would have biased the results considerably, yielding a bulk modulus too high by a factor of 2.

Initially, we conserved the space group symmetries during compression for α-P_3N_5 and γ-P_3N_5 within *C*2/*c* and *Imm*2, respectively. However, we then calculated the bulk modulus for α-P_3N_5 about 30% higher than for the denser phase of γ-P_3N_5—a fact, which made us suspicious. A more detailed analysis, using the option of different settings of the primitive unit cell geometry, revealed a transformation for α-P_3N_5 from *C*2/*c* to *Cc* already at very low pressures. The distance of the N1 atom from the origin (in the space group *C*2/*c* the center of inversion) varies almost linearly with pressure. We have, therefore, dismissed the constraint of a centrosymmetric space group of α-P_3N_5 in all further calculations. The structural transition can also be detected by an inspection of the vibrational spectrum of α-P_3N_5 calculated under pressure. If the space group symmetry *C*2/*c* is retained, the spectrum we obtain at 3 GPa exhibits imaginary eigenfrequencies, and the corresponding eigenvectors indicate the displacement of the N atom from the center of inversion. Therefore, the transition from *C*2/*c* to *Cc* happens between 0 and 3 GPa. It is, however, impossible to locate the pressure of transition more accurately due to the tiny energy differences and forces involved in this gradual transition.

The variation of energy with volume is shown for α-P_3N_5 and γ-P_3N_5 in Figure 4 for both LDA (left side) and GGA (right). α-P_3N_5 clearly is the polymorph of P_3N_5 with lower

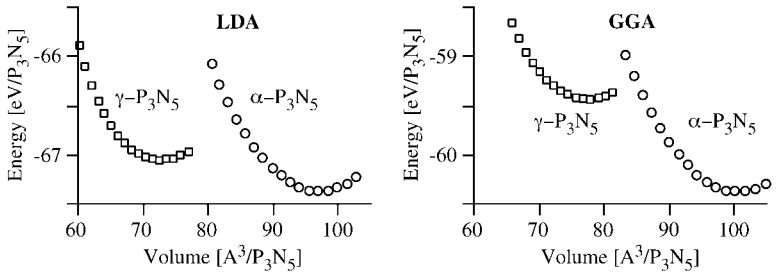

Figure 4. Energy–volume diagram for α-P_3N_5 and γ-P_3N_5. On the left side the results obtained within the LDA; on the right the GGA results. Energy and volume are given per formula unit P_3N_5.

energy, by 0.3 eV/P_3N_5 within LDA and 1 eV/P_3N_5 within GGA. Clearly, LDA and GGA results reveal a certain discrepancy considering the energy differences between the two phases. The GGA results appear to be more reliable in this instance, as we will show when the transition pressure between the two phases is calculated and compared with the experimental results.

We fitted the $E-V$ diagrams of Figure 4 with Murnaghans equation-of-state (EOS) around the minimum to extract the bulk modulus B_0 for both structures. In the case of γ-P_3N_5, this procedure readily provided the results given in in Table 10. On the other had, we encountered some conspicuous problems in the case of α-P_3N_5. Taking volumes ± 4% around the optimized volume of α-P_3N_5, the calculated bulk modulus of α-P_3N_5 is determined to be 20% higher than that of γ-P_3N_5. While this result is not impossible (although unprecedented, to our knowledge), it nevertheless contradicts the expectation of the denser polymorph, namely γ-P_3N_5, being the one with the lower compressibility, and quite often the "harder" one. To elucidate the reliability of the fitting procedure, we

Table 10. Results of a Murnaghan—EOS fit.[a]

	α-P_3N_5		γ-P_3N_5	
	LDA	GGA	LDA	GGA
E_0	−67.36	−60.37	−67.05	−59.43
V_0	96.91	100.48	72.60	77.45
B_0	99	87	116	103
B'	1.9	2.0	5.0	4.5

[a] Energy and volume are given in eV and $Å^3$, respectively. The bulk modulus B_0 for zero pressure is given in GPa. B' is the dimensionless derivative of the bulk modulus at zero pressure.

0947-6539/02/0815-3534 $ 20.00+.50/0 *Chem. Eur. J.* **2002**, *8*, No. 15

recalculated the EOS taking into account only data points of the compressive part of the $E-V$ diagram of α-P_3N_5. This procedure yielded significantly lower values of B_0 for α-P_3N_5 (Table 10); however, these values should be treated with great care. The parameter B' (the dimensionless pressure derivative) of the fit scattered from -4 to 2, depending on the explicit choice of data points. Keeping the parameter $B'=4$ fixed during the fitting yielded even lower values of B_0. We note that Murnaghan's EOS, despite its simplicity, typically describes the compressibility of many compounds up to surprisingly high pressures.[17] Choosing Birch's EOS[18] instead, did not improve the "stability" of our fitting procedure, but yielded values for B_0 of α-P_3N_5 lower by 10%. Interestingly, the bulk modulus calculated for γ-P_3N_5 is almost unaffected (at most by 5%) by the specific choice of EOS or data points.

In the experiment pressure p and temperature T are varied. The thermodynamical variable that governs the transition between phases under equilibrium conditions is the free energy $G=E+pV-TS$. The difference ΔG between two phases constitutes the driving force for a structural transformation. The entropy contribution to ΔG is commonly neglected, due to the small difference in entropy between the crystal structures. Thus, ΔG can be replaced by ΔH, which can be calculated by using $H=E+pV$. The pressure p can be extracted from the $E-V$ graph by a simple numerical differentiation: $p=-\partial E/\partial V$. We chose a spline interpolation function for the $E-V$ data, due to the problems we encountered for α-P_3N_5. Having calculated p and ΔH it is good practice to plot the enthalpy with reference to a given phase, in this case with respect to α-P_3N_5. The resulting enthalpy–pressure ($H-p$) diagram is given in Figure 5. The intersection of the curves for α-P_3N_5 and γ-P_3N_5 indicates the situation when the enthalpy, and thus the free energy in our approximation, of both phases is identical. At higher pressures γ-P_3N_5 has the lower free energy, at lower pressures α-P_3N_5. From Figure 5 we extract a transition pressure for the transition α-$P_3N_5 \rightarrow \gamma$-$P_3N_5$ of 1.9 GPa within the LDA and 6.2 GPa within the GGA. The calculated values are somewhat lower than the experimentally estimated transition pressure. In the experiment the sample was first pressured at room temperature to 11 GPa.[6] At this pressure it was heated over 30 min to 1500 °C, kept at this temperature for 5 min, and quenched to room temperature. The pressure was released gradually over the following 15 h. Therefore, the experiment certainly found an upper boundary for the pressure of the phase transition, while the accurate value yet has to be determined.

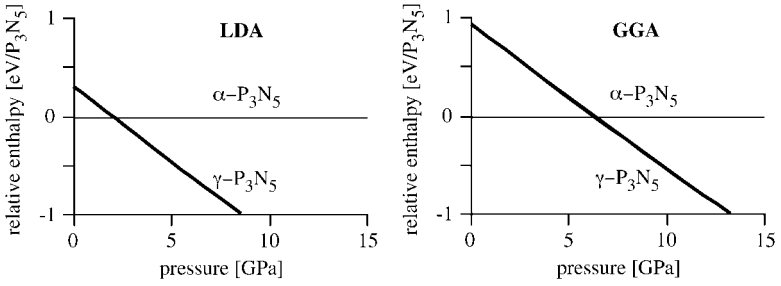

Figure 5. Enthalpy–pressure diagrams for the P_3N_5 system. LDA (left) and GGA (right) results. In both cases the enthalpy is given per formula unit P_3N_5 relative to that of α-P_3N_5.

Further high-pressure phases of P_3N_5: The recent developments of high-pressure experimental techniques have revealed a wealth of new information about the behavior of materials. The structure of γ-P_3N_5 suggests the possibility of finding an even higher coordinated polymorph of P_3N_5. The N1 atom might shift towards the P2 atoms to complete the octahedron around P2. We tested for this additional structural change by applying extreme pressures up to 200 GPa and by building the suspected geometry from scratch; however, we encountered no structural transition within the chosen unit cell.

In the course of searching for possible structural candidates for a δ-P_3N_5 we considered the structures of Ta_3N_5, and several silicates of appropriate composition. All structures we considered comprise a higher average coordination than γ-P_3N_5. Compounds such as Al_2SiO_5 and MSi_2O_5 (M = Mg,Ca) display a rich high-pressure chemistry, and adopt structure types with pentahedrally and octahedrally coordinated cations.[22, 23] However, almost all structure types we investigated for a high-pressure phase of P_3N_5 distorted towards lower average coordination, even at higher pressures. A good example for this is the titanite structure type. Some candidate structures which initially appeared appealing because of their lower unit cell volume in comparison to γ-P_3N_5, proved unsuitable under pressure, presumably due to an unfavorable arrangement of anions.

The most promising candidate that we found for a δ-P_3N_5 phase is isotypic to kyanite, an Al_2SiO_5 modification.[19] The structure, which has the space group symmetry $P\bar{1}$, is shown in Figure 6. It comprises edge-sharing $\{\mathbf{P}\}N_6$ octahedra, while isolated $\{\mathbf{P}\}N_4$ tetrahedra share vertices with the octahedra. This situation is thus very similar to that found in spinels (A_2BO_4). Unfortunately, we were not able to calculate a hypothetical spinelloid P_3N_5 with a cubic closed packed anion array, due to the explicit composition P_3N_5.

As before, we calculated the variation of the energy with respect to the volume of the unit cell of δ-P_3N_5. Figure 7 shows the $E-V$ diagram for γ-P_3N_5 and δ-P_3N_5, which indeed indicates a phase transition between both polymorphs. The enthalpy–pressure diagram, with ΔH given relative to γ-P_3N_5, is given on the right side of Figure 7. From this graph we extract the transition pressure p_t for the transition γ-P_3N_5 to δ-P_3N_5 to be 43 GPa within the GGA, while calculations within the LDA yield a value of 28 GPa. A further high-pressure phase of phosphorus nitride, therefore, should appear at significantly lower pressures than we recently proposed for a post-spinel modification of Si_3N_4 or Ge_3N_4 ($\approx$150 GPa).[24] The structural data of the triclinic δ-P_3N_5 at 43 GPa is given in Table 11 and Table 12.

The kyanite structure of P_3N_5 might, however, not be stable at

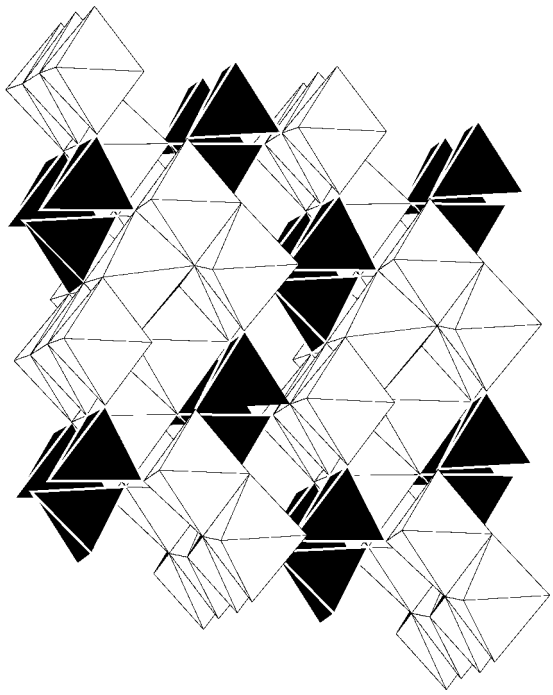

Figure 6. Hypothetical δ-P_3N_5 with kyanite structure. {**P**}N_6 octahedra are hatched, {**P**}N_4 tetrahedra are colored black.

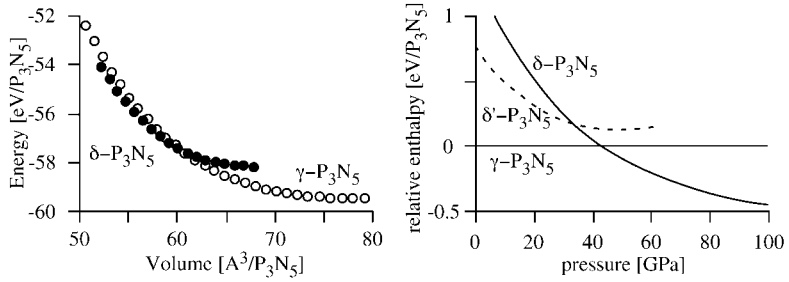

Figure 7. Left: $E-V$ diagram for γ-P_3N_5 and δ-P_3N_5 within the kyanite structure. Right: $\Delta H-p$ of δ-P_3N_5 relative to γ-P_3N_5. The dashed line corresponds to the monoclinic structure of δ' (see text for details).

Table 11. Structural data of δ-P_3N_5 (at 43 GPa) and δ'-P_3N_5 (for ambient pressure) calculated within the LDA. The volume is given per formula unit P_3N_5. Note that we used the standard setting of δ'-P_3N_5. The relation to the Kyanite structure becomes apparent if the non-standard setting $P112_1/m$ is used.

	δ-P_3N_5	δ'-P_3N_5
space group (no.)	$P\bar{1}$ (2)	$P2_1/m$ (11)
a [Å]	6.6026	6.8054
b [Å]	7.1731	5.3863
c [Å]	5.1076	7.6543
α	89.6	90.0
β	101.1	106.4
γ	105.8	90.0
V [Å^3]	57.0	67.3

lower pressures. Though we could quench it to zero pressure, a slight expansion of the volume resulted in a more symmetric monoclinic structure, denoted as δ'-P_3N_5, with significantly lower energy. An inspection of the respective enthalpy curves given in Figure 7 reveals that δ'-P_3N_5 undergoes a transition to the kyanite structure (δ-P_3N_5) at about 34 GPa. Since both modifications, the monoclinic and the triclinic structure, are

Table 12. Atomic positions of δ-P_3N_5 calculated at 43 GPa within the LDA.

Atom	x	y	z
P1	0.3246	0.7057	0.4564
P2	0.3047	0.7020	0.9517
P3	0.1106	0.3880	0.6416
P4	0.1113	0.9173	0.1652
P5	0.2986	0.0680	0.7060
P6	0.2943	0.3291	0.1903
N1	0.0969	0.1422	0.1287
N2	0.5072	0.2501	0.7567
N3	0.1181	0.6788	0.1780
N4	0.2811	0.4591	0.9417
N5	0.2889	0.9346	0.9524
N6	0.0969	0.1543	0.6554
N7	0.1163	0.6320	0.6393
N8	0.2895	0.4525	0.4414
N9	0.2969	0.9430	0.4547
N10	0.5076	0.2590	0.2481

related by a shear distortion, this transition appears likely to happen during the process of quenching. The $H-p$ curve of the monoclinic δ'-P_3N_5, however, does not cross the $H-p$ curve of γ-P_3N_5. δ'-P_3N_5 thus should not be considered a possible high-pressure phase of P_3N_5. The structural data of δ'-P_3N_5, for which we used the standard setting in space group $P2_1/m$, are included in Table 11 and atomic positions are given in Table 13. δ'-P_3N_5 comprises {**P**}N_6 octahedra, {**P**}N_5 trigonal bipyramids, and {**P**}N_4 tetrahedra. It is, however, not structurally related to any of the Ca-Si_2O_5 polymorphs. The compressibility of δ'-P_3N_5 is significantly lower than that of γ-P_3N_5, which is presumably attributed to the higher average coordination of atoms in δ'-P_3N_5. We calculated the zero pressure bulk modulus of δ'-P_3N_5 to 240 GPa and its derivative to 4.0. This value of B_0 is more than twice as much as for γ-P_3N_5 and is comparable to the bulk modulus of β-Si_3N_4, for which values of about 250 GPa have been determined experimentally[25] and theoretically.[4]

Table 13. Atomic positions of δ'-P_3N_5 (at ambient pressure) in space group $P2_1/m$ calculated within the LDA.

Atom	x	y	z
P1	0.3092	0.5068	0.6992
P2	0.1368	¾	0.3991
P3	0.1403	¼	0.9387
P4	0.3021	¾	0.0669
P5	0.2889	¼	0.3213
N1	0.1177	¼	0.1401
N2	0.5104	¼	0.2720
N3	0.5139	¾	0.2394
N4	0.1300	¼	0.6918
N5	0.2724	0.0136	0.4528
N6	0.2804	0.9893	0.9325
N7	0.1162	¾	0.1659
N8	0.1369	¾	0.6248

0947-6539/02/0815-3536 $ 20.00+.50/0 *Chem. Eur. J.* **2002**, *8*, No. 15

Many high-pressure phases of ternary materials decompose into phase assemblages of binary compounds on further compression.[22] For binary P_3N_5 such a pathway evidently is not possible. However, to access the relevance of δ-P_3N_5 within the P–N phase diagram we calculated the enthalpy for the decomposition reaction of P_3N_5 into its elemental constituents, phosphorus, and nitrogen, as a function of pressure. Within the pressure range from 10 GPa to 40 GPa phosphorus adopts a simple cubic structure.[26] Nitrogen, as a gaseous element at ambient conditions, can be solidified at low temperatures, and its phase diagram is a topic of current research.[27, 28, 29] We chose to calculate the diatomic ε-phase of N_2, since the δ- and ζ-phases differ only in the orientation of the molecules and, hence, any energy difference is very small. In addition, we inspected the polymeric cubic phase of nitrogen. The enthalpy difference between binary P_3N_5 and the elemental high-pressure phases of P and N was found to be larger than 2 eV at zero temperature for the whole pressure regime up to 100 GPa, therefore, clearly favoring the binary compound. Within the given limitations—as we cannot access the contributions of entropy at elevated temperatures to the free energy of the decomposition—we conclude that the appearance of a further high-pressure phase of P_3N_5 is very likely—or that the P–N phase diagram might offer some "new chemistry".

Summary

Applying DFT methods for the investigation of phosphorus nitride, P_3N_5, provides a consistent picture for the structures α-P_3N_5 and γ-P_3N_5. Taking the typical trends of LDA and GGA calculations into account, both approximations yield almost identical results for atomic positions, cell geometry, and compressibility. We found the space group symmetry of α-P_3N_5 at ambient pressures to be *C*2/*c*. The zone-center phonon modes calculated within the LDA compare very well with the experimental results and indicate low-frequency bending modes for the two-coordinated N atoms, which are responsible for a structural instability of α-P_3N_5 at higher pressures. α-P_3N_5, with a bulk modulus of approximately 100 GPa, is less compressible than γ-P_3N_5, for which we calculated a bulk modulus of 116 GPa within the LDA. GGA calculations are, however, superior for the estimation of transition pressures between phases of different coordination. We found within the GGA that α-P_3N_5 should transform into γ-P_3N_5 at pressures of about 6–7 GPa, which is close to the upper boundary of 11 GPa determined experimentally. At significantly higher pressures of about 40 GPa we expect P_3N_5 to transform into a triclinic δ-P_3N_5 phase with a kyanite-type structure. This triclinic modification of P_3N_5 might, however, undergo a shear distortion during the quenching to lower pressures towards a more symmetrical monoclinic phase.

Acknowledgements

The authors gratefully acknowledge the generous support by the Deutsche Forschungsgemeinschaft (DFG) and by the Fonds der Chemischen Industrie (FCI).

[1] W. Schnick, *Angew. Chem.* **1993**, *105*, 846; *Angew. Chem. Int. Ed. Engl.* **1993**, *32*, 806.
[2] S. Horstmann, E. Irran, W. Schnick, *Angew. Chem.* **1997**, *109*, 1938; *Angew. Chem. Int. Ed. Engl.* **1997**, *36*, 1873.
[3] S. Horstmann, E. Irran, W. Schnick, *Z. Anorg. Allg. Chem.* **1998**, *624*, 620.
[4] A. Zerr, G. Miehe, G. Serghiou, M. Schwarz, E. Kroke, R. Riedel, H. Fueß, P. Kroll, R. Boehler, *Nature* **1999**, *400*, 340.
[5] M. Schwarz, G. Miehe, A. Zerr, E. Kroke, B. Poe, H. Fuess, R. Riedel, *Adv. Mater.* **2000**, *12*, 883.
[6] K. Landskron, H. Huppertz, J. Senker, W. Schnick, *Angew. Chem.* **2001**, *113*, 2713; *Angew. Chem. Int. Ed.* **2001**, *40*, 2643.
[7] J. V. Badding, *Annu. Rev. Mater. Sci.* **1998**, *28*, 631..
[8] T. Sekine, in *High-Pressure Shock Compression of Solids IV* (Eds.: L. Davison, Y. Horie), Springer, New York **1997**.
[9] P. Hohenberg, W. Kohn, *Phys. Rev. A* **1964**, *136*, 864.
[10] G. Kresse, J. Hafner, *Phys. Rev. B* **1993**, *47*, 558; G. Kresse, J. Hafner, *Phys. Rev. B* **1994**, *49*, 14251.
[11] G. Kresse, J. Furthmüller, *Comput. Mat. Sci.* **1996**, *6*, 15.
[12] G. Kresse, J. Furthmüller, *Phys. Rev. B* **1996**, *55*, 11169.
[13] J. P. Perdew, A. Zunger, *Phys. Rev. B* **1981**, *23*, 5048.
[14] D. M. Ceperley, B. J. Alder, *Phys. Rev. Lett.* **1980**, *45*, 1814.
[15] J. P. Perdew in *Electronic Structure of Solids '91* (Eds.: P. Ziesche, H. Eschrig), Akademie Verlag, Berlin **1991**.
[16] H. J. Monkhorst, J. D. Pack, *Phys. Rev. B* **1976**, *13*, 5188.
[17] O. L. Anderson, *Equation of state of solids for geophysics and ceramic science*, Oxford University Press, New York **1995**.
[18] F. Birch, *J. Geophys. Res.* **1952**, *57*, 227.
[19] C. W. Burnham, *Z. Kristall.* **1963**, *118*, 337.
[20] W. Kleber, K.-T. Wilke, *Krist. Tech.* **1969** , *4*, 165.
[21] P. Kroll, R. Riedel, R. Hoffmann, *Phys. Rev. B* **1999**, *60*, 3126.
[22] L.-G. Liu, W. A. Basset, *Elements, Oxides, and Silicates*, Oxford University Press, New York **1986**.
[23] R. J. Angel, N. L. Ross, F. Seifert, T. F. Fliervoet, *Nature* **1996**, *384*, 441.
[24] P. Kroll, J. von Appen, *Phys. Stat. Sol. (B)* **2001**, *226*, R6.
[25] L. Cartz, J. D. Jorgensen, *J. Appl. Phys.* **1981**, *52*, 236.
[26] J. C. Jamieson, *Science* **1963**, *139*, 129.
[27] E. Gregoryanz, A. F. Goncharov, R. J. Hemley, Ho-K. Mao, *Phys. Rev. B* **2001**, *64*, 052103/1.
[28] R. Bini, L. Ulivi, J, Kreutz, H. J. Jodl, *J. Chem. Phys.* **2000**, *112*, 8522.
[29] C. Mailhiot, L. H. Yang, A. K. McMahan, *Phys. Rev. B* **1992**, *46*, 14419.

Received: March 7
Revised: June 3, 2002 [F3931]